71th International Astronautical Congress (IAC) – The CyberSpace Edition, 12-14 October 2020.

IAC-20,D1,3,5,x56351

Magnetic buoyancy-based water electrolysis in zero-gravity

Á. Romero-Calvo[1], G. Cano-Gómez[2], H. Schaub[3]

The management of fluids in space is complicated by the absence of strong buoyancy forces. This raises significant technical issues for two-phase flows applications, such as water electrolysis or boiling. Different approaches have been proposed and tested to induce phase separation in low-gravity; however, further efforts are still required to develop efficient, reliable, and safe devices. The employment of magnetic buoyancy is proposed as a complement or substitution of current methods, and as a way to induce the early detachment of gas bubbles from their nucleation surfaces. The governing magnetohydrodynamic equations describing incompressible two-phase flows subjected to static magnetic fields in low-gravity are presented, and numerical simulations are employed to demonstrate the reachability of current magnets under different configurations. The results support the employment of new-generation neodymium magnets for centimeter-scale electrolysis and phase separation technologies in space, that would benefit from reduced complexity, mass, and power requirements.

1 Introduction

The term *water electrolysis* refers to the electrically induced decomposition of water into oxygen and hydrogen. The reaction was first performed by Troostwijk and Deiman in 1789 [1, 2], and has been considered for space applications since the early 1960s [3]. A wide range of environmental control and life support systems [4], propulsion technologies [5–7], or energy conversion and storage mechanisms [8, 9] rely on this process. Furthermore, future interplanetary missions are likely to employ water as an In-Situ-Resource-Utilization propellant [10, 11].

The operation of electrolytic cells in low-gravity is severely complicated by the absence of strong buoyancy forces, commonly resulting in increased complexity, mass, and power consumption. Dedicated microgravity experiments have shown how the weak buoyancy force gives rise to a layer of gas bubbles over the electrodes, shielding the active surface and increasing the ohmic resistance [12–14]. Gas bubbles tend to be larger than in normal-gravity conditions due to the longer residence time on the electrodes and the absence of bubble departure. Besides, and unlike in normal-gravity, the bubble departure diameter increases with increasing current intensity [15]. A forced water flow can be employed to flush this structure, but this approach increases the complexity of the system and has a limited efficiency [16]. Most types of electrolytic cells also require a liquid/gas phase separation stage. Rotary [17, 18] and membrane-type [16, 19] devices are nowadays employed. Passive approaches that make use of surface tension by means wedge geometries [20, 21], springs [22], or eccentric annuli [23] have also been proposed and tested. As an alternative, the generation of an equivalent buoyancy force by means of electric fields has been considered since the early 1960s [24] and has been studied and successfully tested for low-gravity boiling [25, 26] and two-phase flow [27, 28] applications. However, the drawbacks of these approaches are numerous: centrifuges add to system power loads and may represent a safety hazard, membranes have limited lifetime and tend to clog in the presence of water impurities [5, 29], surface tension-based approaches require careful geometrical design and are sensitive to moderate departures from the operational design point [20], and electric fields consume power and may represent a safety hazard for both human and autonomous spaceflight due to the large required potential differences.

This review unveils the numerous challenges associated with the low-gravity gas/liquid separation process and shows important limitations in current and foreseen technologies. As a complement or substitution of the previous methods, the inherent magnetic properties of water and derived electrolytes may be employed to induce the natural detachment and collection of gas bubbles. Inhomogeneous magnetic fields induce a weak body force that, due to the differential magnetic properties between phases, results in a net buoyancy force [30]. This phenomenon is known as *magnetic buoyancy* and has been applied to terrestrial boiling experiments with ferrofluids [31, 32]. Previous works on low-gravity magnetohydrodynamics have explored the diamagnetic manipulation of air bubbles in water [33, 34], the positioning of diamagnetic materials [35], air-water separation [36], protein crystal growth [37], magnetic positive positioning [38–42], magnetic liquid sloshing [43, 44], or combustion enhancement [34], among others. The application of Lorentz's force on liquid electrolytes has also been studied as a way to enhance hydrogen production [45–55]. However, the use of magnetic buoyancy in phase separation, electrolysis, and boiling in low-gravity remains largely unexplored.

The development of low-gravity magnetic phase separators may lead to reliable, lightweight, and passive devices. If the magnetic force was applied directly over the electrodes, the bubble departure diameter would be reduced and a convective flow would be induced on the layer of bubbles, enlarging the effective electrode surface and minimizing the ohmic resistance and cell voltage. The same benefits would be obtained for low-gravity boiling devices, with the boiling surfaces being equivalent to the electrodes.

In this paper, the applications of magnetic buoyancy in low-gravity electrolysis are first explored in Sec. 2. A theoretical framework for incompressible liquids subjected to static magnetic fields is derived Sec. 3, while a preliminary analysis of bubble dynamics is given in Sec. 4. Fundamental results and technical solutions are shown in Sec. 5, and conclusions are finally drawn in Sec. 6.

[1]Department of Aerospace Engineering Sciences, University of Colorado Boulder, CO, United States; alvaro.romerocalvo@colorado.edu
[2]Departamento de Física Aplicada III, Universidad de Sevilla, Sevilla, Spain; gabriel@us.es
[3]Department of Aerospace Engineering Sciences, University of Colorado Boulder, CO, United States; hanspeter.schaub@colorado.edu

2 Magnetic buoyancy applications to low-gravity water electrolysis

Water electrolysis technologies can be classified according to the nature of the electrolyte. Liquid electrolyte assemblies, known as alkaline cells, employ two metallic electrodes separated by a porous material and immersed in a conductive aqueous solution, usually prepared with KOH or $NaOH$. The cell separator, which is either attached to the electrodes (zero-gap configuration) or slightly separated from them (gap-cell configuration) allows the exchange of the OH^- groups and prevents the recombination of H_2 and O_2 into water. Solid electrolytes, or Proton-Exchange Membrane (PEM) cells, on the contrary, are fed with pure water and make use of a proton-conducting polymer electrolyte attached to two electrodes in a zero-gap configuration. PEM cells minimize ohmic losses, allow high current densities, prevent the recombination of oxygen and hydrogen (and so, are safer), and produce high-purity gases. However, they lack the long-term heritage of alkaline cells and are sensitive to water impurities [56]. These and alternative approaches have already been tested in space [57–59].

The application of magnetic buoyancy may be beneficial for at least two common components of low-gravity water electrolysis systems: the electrolytic cell and the gas/liquid phase separator. These elements are present in both alkaline and PEM cells, with the exception of SFWES configurations. As shown in Sec. 3.4, magnetic buoyancy can be induced in virtually all liquids of technical interest, with pure water being one of the least magnetically susceptible of them. Although this discussion focuses on water electrolysis, the concepts here introduced have a direct equivalent in applications involving pool boiling or bubble growth, such as water boiling or other types of electrolysis, recombination, or combustion reactions.

2.1 *Electrolytic cells*

The application of strong inhomogeneous magnetic fields over the electrodes would potentially induce a convective flow on the layer of bubbles, reducing the break-off diameter, enlarging the effective surface, minimizing the ohmic resistance, and reducing the cell voltage while effectively separating the phases. Some of these effects have been observed in terrestial boiling experiments with ferrofluids, where a significant influence of the magnetic field on the boiling plate bubble coverage and heat transfer coefficient is reported [31, 32].

Depending on the type of reactant, the diamagnetic or para/ferromagnetic configurations depicted in Fig. 1 should be considered. While in the former a diamagnetic liquid (such as water) is repelled from the magnet, in the latter a paramagnetic or ferromagnetic substance is employed, producing the opposite effect. In virtue of Archimedes' principle, gas bubbles experience a magnetic buoyancy force that attracts (diamagnetic) or expels (para/ferromagnetic) them from the magnet.

This distinction may sound contrived to the reader, as water and its associated electrolytes are diamagnetic materials, and one cannot easily figure out applications where paramagnetic or ferromagnetic substances are employed. However, the renewed interest in nanofluids-enhanced [60] and magnetically-enhanced [31, 32] heat transfer may open new interesting avenues of research. Highly susceptible liquids, such as ferrofluids, may be employed to boost the productivity of the electrodes and boiling surfaces, both on Earth and in space. In spite of the numerous technical challenges that such technologies would face (e.g. thermal stability and particle deposition [61]), the possibility of using ferrofluids is considered in this work.

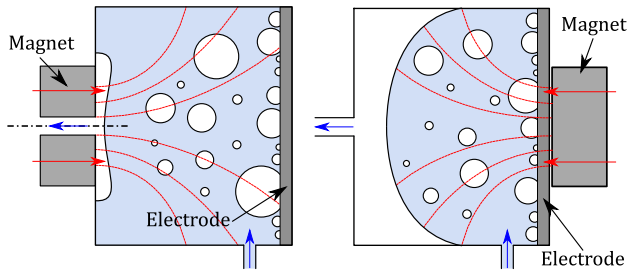

(a) Diamagnetic (b) Para/Ferromagnetic

Fig. 1: Conceptual representation of a magnetically enhanced electrolysis cell. Blue arrows represent the liquid/gas flow, while red arrows denote the magnetization vector.

2.2 *Phase separators*

Although the magnetic electrolytic cell concept presents intrinsic advantages, modularity is commonly sought in an industry characterized by a complicated and expensive design flow. Magnetic phase separators could be easily integrated in existing space systems, with applications to any combination of phases. The magnetic buoyancy force could also be employed in combination with existing technologies, such as surface-tension enabled phase separators.

This is conceptually represented in Fig. 2, where magnetic and combined surface tension/magnetic phase separators are shown for a dielectric liquid. The magnetic phase separator consists on a channel surrounding a magnet that attracts the bubbles from an incoming two-phase flow. The combined phase separator consists on a wedge-shaped channel that pushes large bubbles to the open end as they evolve towards their configuration of minimum energy (spherical geometry). This approach was tested in the Capillary Channel Flow experiment, conducted at the ISS in April 2010 [20]. Mag-

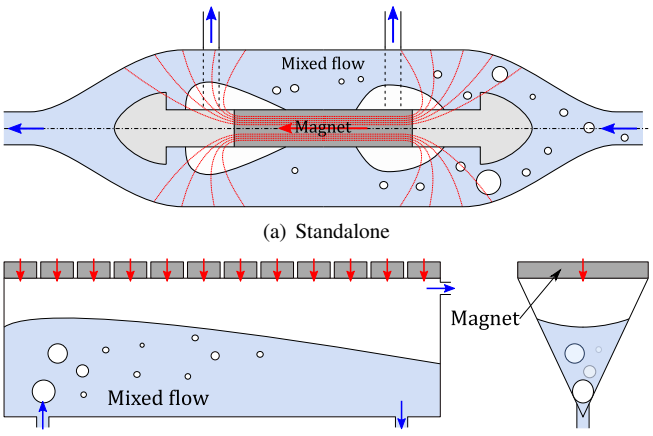

(a) Standalone

(b) Combined

Fig. 2: Conceptual representation of a standalone and surface-tension enhanced diamagnetic phase separator. Blue arrows represent the liquid/gas flow, while red arrows denote the magnetization vector.

netic buoyancy may be particularly useful to attract small bubbles that are unlikely to contact the free surface and hence remain within the liquid flow.

3 Magnetic buoyancy in two-phase flows

The conceptual solutions here presented should be studied in the framework of the magnetohydrodynamic theory. This section introduces a series of fundamental theoretical tools together with simplified expressions that enable preliminary analyses. Due to their potential interest in future applications, the use of ferrofluids is considered. No assumptions are made regarding the constitutive relation of the material.

3.1 Governing equations for incompressible, neutral fluids subjected to static magnetic fields

The magnetic phase separation and bubble detachment concept discussed in this paper can be applied to different electrolysis and boiling technologies. However, most of them share three important characteristics: (i) the fluids involved are incompressible and electrically neutral, (ii) steady magnetic fields are imposed, and (iii) viscous coefficients are constant. Under the previous assumptions, the magnetohydrodynamic mass and momentum conservation equations are expressed as [62]

$$\nabla \cdot \boldsymbol{v} = 0, \tag{1a}$$

$$\rho \frac{D\boldsymbol{v}}{Dt} = \rho \boldsymbol{g} + \nabla \cdot \mathrm{T}, \tag{1b}$$

subjected to appropriate boundary conditions, with $\boldsymbol{v}$ being the velocity field, ρ the fluid density, $\boldsymbol{g}$ the inertial acceleration, D/Dt the material derivative, and T the Maxwell stress tensor, that includes pressure, viscous, and magnetic terms.

The stress tensor T is defined in terms of the magnetic fields acting on the system. Those are computed from the stationary Maxwell equations in the absence of electric charges

$$\nabla \cdot \boldsymbol{B} = \boldsymbol{0}, \tag{2a}$$

$$\nabla \times \boldsymbol{H} = \boldsymbol{0}, \tag{2b}$$

where $\boldsymbol{B}$, $\boldsymbol{H} = (\boldsymbol{B}/\mu_0) - \boldsymbol{M}$, and $\boldsymbol{M}$ are the flux density, magnetic, and magnetization fields, respectively, and μ_0 is the permeability of vacuum. For soft magnetic materials, the magnetization field is aligned with the magnetic field and follows the relation $\boldsymbol{M} = \chi^{\mathrm{vol}}(H)\boldsymbol{H}$, with $\chi^{\mathrm{vol}}(H)$ being the volume magnetic susceptibility. The interfacial magnetic boundary conditions are

$$\boldsymbol{n} \cdot (\boldsymbol{B}_2 - \boldsymbol{B}_1) = 0, \tag{3a}$$

$$\boldsymbol{n} \times (\boldsymbol{H}_2 - \boldsymbol{H}_1) = 0. \tag{3b}$$

Therefore, the normal component of $\boldsymbol{B}$ and, in the absence of surface currents, the tangential component of $\boldsymbol{H}$, are continuous across the interface.

This theoretical framework can be further simplified when considering linear dia/paramagnetic materials, which exhibit a constant (magnetic field independent) susceptibility of the order $|\chi^{vol}| \ll 1$. Consequently, the weak magnetization field in this media justifies the approximation $\boldsymbol{H} \approx \boldsymbol{H}_0$, with $\boldsymbol{H}_0$ being the *applied* magnetic field. From a practical perspective, this implies that $\boldsymbol{H}_0$ can be calculated independently of the state of the system under analysis.

3.2 The incompressible, viscous Maxwell stress tensor

The magnetodynamic state of an incompressible continuous medium can be described by means of the viscous Maxwell stress tensor, which has been formulated in the classical literature as [30, 62–64]

$$\mathrm{T} = \mathrm{T}_p + \mathrm{T}_\nu + \mathrm{T}_m, \tag{4}$$

with the pressure, viscous, and magnetic terms being given by

$$\mathrm{T}_p = -p^* \ \boldsymbol{I}, \tag{5a}$$

$$\mathrm{T}_\nu = \eta \left[\nabla \boldsymbol{v} + (\nabla \boldsymbol{v})^T \right], \tag{5b}$$

$$\mathrm{T}_m = -\frac{\mu_0}{2} H^2 \boldsymbol{I} + \boldsymbol{B}\boldsymbol{H}, \tag{5c}$$

and where

$$p^* = p(\nu, T) + \mu_0 \int_0^H \frac{\partial}{\partial \nu} \left[\nu M\right] dH' \tag{6}$$

is the *composite pressure*, that includes hydrostatic $p(\nu, T)$ and magnetopolarization terms. In the previous expressions, $\boldsymbol{I} = \delta_{ij}\boldsymbol{e}_i\boldsymbol{e}_j$ is the unit dyadic in the Cartessian $\boldsymbol{e}_i$ reference system, and $\nu = \rho^{-1}$ is the specific volume of the medium. η is the dynamic coefficient of viscosity, that shows a nonlinear dependence with the magnetic field for ferrofluids [65]. Applications involving unequilibrated ferrofluid solutions (i.e. those for which $\boldsymbol{M} \times \boldsymbol{H} \neq 0$), should incorporate the effects resulting from particle rotation in a viscous carrier liquid. An additional term should be added to the viscous stress tensor T_ν, and the angular momentum and magnetic relaxation equations should be considered [62, 64].

The electric interaction has been widely studied in the context of two-phase flows [27] and does not have a significant incidence for the applications discussed in this work. Even though the small differential electrode potential employed in water electrolysis cells ($\approx$ 3 V) produces an electric field, the density of electric force exerted on the electrically polarized medium would be several orders of magnitude weaker than its magnetic counterpart. Consequently, this discussion focuses on the magnetohydrodynamic effect by assuming an electrically neutral medium that remains in thermodynamic equilibrium with constant density, temperature and chemical potentials.

This formulation does not implement any assumption regarding the constitutive relation of the material. In some cases, however, it may be useful to particularize the analysis to linear media, neglecting the magnetopolarization term in Eq. 6. Linear electric results are introduced in Ref. 27 and can be easily adapted to the dia/paramagnetic case by making use of the complete analogy between magnetostatics and electrostatics [30].

3.2.1 Body force distributions

The forces per unit volume exerted on the medium in the absence of electric fields can be computed as the divergence of the stress tensor given by Eq. 4, resulting in [62]

$$\boldsymbol{f} = \nabla \cdot \mathrm{T} = \boldsymbol{f}_p + \boldsymbol{f}_\nu + \boldsymbol{f}_m \tag{7}$$

with

$$\boldsymbol{f}_p = \nabla \cdot \mathrm{T}_p = -\nabla p^*, \tag{8a}$$

$$\boldsymbol{f}_\nu = \nabla \cdot \mathrm{T}_\nu = \nabla \cdot \left\{ \eta \left[\nabla \boldsymbol{v} + (\nabla \boldsymbol{v})^T \right] \right\}, \quad (8b)$$

$$\boldsymbol{f}_m = \nabla \cdot \mathrm{T}_m = \mu_0 M \nabla H. \quad (8c)$$

If the viscosity coefficient η is considered constant, the viscous term reduces to

$$\boldsymbol{f}_\nu = \eta \nabla^2 \boldsymbol{v} + \eta \nabla (\nabla \cdot \boldsymbol{v}).$$

3.2.2 Boundary conditions

Surface forces appear in the interface between immiscible media as a consequence of the discontinuity in the stress tensor. Those forces are balanced according to the condition of stress equilibrium, leading to [62]

$$\boldsymbol{t}_{n,2} - \boldsymbol{t}_{n,1} = 2\sigma \mathcal{H} \boldsymbol{n}_1, \quad (9)$$

where $\boldsymbol{t}_{n,i} = \boldsymbol{n}_i \cdot \mathrm{T}_{m,i}$ is the stress vector, $\boldsymbol{n}_i$ is the external normal of the medium i, the right term is the *capillary pressure*, σ is the surface tension, and $\mathcal{H}$ is the mean curvature of the interface. Implementing the magnetic, viscous stress tensor given by Eq. 4, the stress vector is expressed as

$$\boldsymbol{t}_n = -p^* \boldsymbol{n} + \eta \left[2 \frac{\partial v_n}{\partial x_n} \boldsymbol{n} + \left(\frac{\partial v_n}{\partial x_t} + \frac{\partial v_t}{\partial x_n} \right) \boldsymbol{t} \right] - \frac{\mu_0}{2} H^2 \boldsymbol{n} + B_n \boldsymbol{H}, \quad (10)$$

where v_n and v_t are the normal and tangential velocity components, and x_n and x_t the distances along the normal and tangential directions, respectively. Computing the balance at the interface, considering Gauss' and Ampère's laws, and expressing the result in the normal (n) and tangential (t) directions, the *ferrohydrodynamic (FHD) viscous boundary condition* is obtained [62]

$$n: \quad \left[p^* - 2\eta \frac{\partial v_n}{\partial x_n} + p_n \right] + 2\sigma \mathcal{H} = 0, \quad (11a)$$

$$t: \quad \left[\eta \left(\frac{\partial v_n}{\partial x_t} + \frac{\partial v_t}{\partial x_n} \right) \right] = 0, \quad (11b)$$

with $p_{n,i} = \mu_0 M_{n,i}^2 / 2$ being a pressure-like term named *magnetic normal traction*, and the brackets denoting a difference across the interface. If the second medium is nonmagnetic and viscosity is neglected, the normal balance reduces to the inviscid boundary condition between magnetizable and nonmagnetizable media obtained in Ref. 65, as it should.

3.3 Effective total forces

As shown in Ref. 66, different equivalent formulations can be employed to compute the total magnetic force exerted on a body. Among them, the Principle of Virtual Works can be applied to the free energy variation of a magnetizable medium caused by changes in the external magnetic field $\boldsymbol{H}_0$. The result is a well-known and straightforward expression [30, 63, 66]. After considering the quasistatic momentum balance arising from Eq. 1b, the *effective total magnetic force* becomes

$$\boldsymbol{F}_m^{\text{eff}} = \mu_0 \int_V \mathrm{d}V \ \left[(\chi_b^{\text{vol}} \boldsymbol{H} - \chi_e^{\text{vol}} \boldsymbol{H}^*) \cdot \nabla \right] \boldsymbol{H}_0, \quad (12)$$

where V denotes the volume and surface of a magnetized medium, respectively, and with $\boldsymbol{H}^*$ being the *virtual* magnetic field that would be present if the volume V was occupied by the environment. This expression constitutes the formulation of the Archimedes' principle for the magnetic interaction. By following the same procedure, the effective inertial force can be obtained as

$$\boldsymbol{F}_{\text{in}}^{\text{eff}} = \int_V \mathrm{d}V \ (\rho_b - \rho_e) \boldsymbol{g} \quad (13)$$

3.4 Magnetic susceptibility

The magnetic susceptibility is an intrinsic property of the medium that defines the relation between the fields $\boldsymbol{M}$ and $\boldsymbol{H}$, which are aligned in soft magnetic materials. Diamagnetic and paramagnetic substances generally have small and constant volume susceptibilities values. Ferrofluids, on the contrary, are characterized by large susceptibilities and a non-linear dependence between $\boldsymbol{M}$ and $\boldsymbol{H}$. Magnetic susceptibilities are commonly expressed per unit volume (χ^{vol}), mass (χ^{mass}), or mole (χ^{mol}) in the international or CGS systems [67].

Since KOH and $NaOH$ solutions are widely employed in water electrolysis technologies, a brief analysis of their magnetic susceptibility is here presented. Assuming that dipole-dipole interactions are negligible, Wiedemann's additivity law states that

$$\chi_{\text{sol}}^{\text{mass}} = \sum_{i=1}^{N} p_i \chi_i^{\text{mass}}, \quad (14)$$

where χ_{sol}^{mass} is the mass susceptibility of the solution, and p_i is the mass fraction of each substance. Equivalent expressions are found for volume and molar susceptibilities [67]. The magnetic susceptibility of diluted salts can be computed as [68]

$$\chi_{\text{salt}}^{\text{mass}} = \frac{\chi_{\text{cation}}^{\text{mol}} + \chi_{\text{anion}}^{\text{mol}}}{\mathcal{M}_{\text{salt}}}, \quad (15)$$

with $\mathcal{M}_{\text{salt}}$ being the molar mass of the salt. The susceptibilities of the ions are expressed per unit mole, as commonly reported in the literature. Values for KOH and $NaOH$ solutions are given in Table 1.

The approximate evolution of the magnetic susceptibility of KOH and $NaOH$ solutions with the solute mass fraction is reported in Fig. 3, where the solubility of the solutions is taken from Ref. 70 at 25° C and a constant solution volume is assumed. Since the magnetic force is directly proportional to the magnetic susceptibility, this result implies that liquid electrolytes are particularly well suited for magnetic buoyancy applications, with increases of magnetic susceptibility of up to an 80%.

4 Bubble dynamics

The magnetic buoyancy force can produce significant effects in the generation and evolution of gas bubbles over electrodes or boiling surfaces. Such effects have been observed in experiments involving electric fields [26] and ferrofluids subjected to magnetic fields [31,

Tab. 1: Relevant magnetic parameters of common water electrolytes expressed in the CGS system [68, 69].

Solute	$\mathcal{M}_{\text{solute}}$ [g/mol]	$\chi_{\text{cation}}^{\text{mol}}/10^{-6}$ [cm^3/mol]	$\chi_{OH^-}^{\text{mol}}/10^{-6}$ [cm^3/mol]	$\chi_{H_2O}^{\text{mass}}/10^{-6}$ [cm^3/g]
NaOH	39.9971	-6.8	-12	-0.720
KOH	56.1056	-14.9		

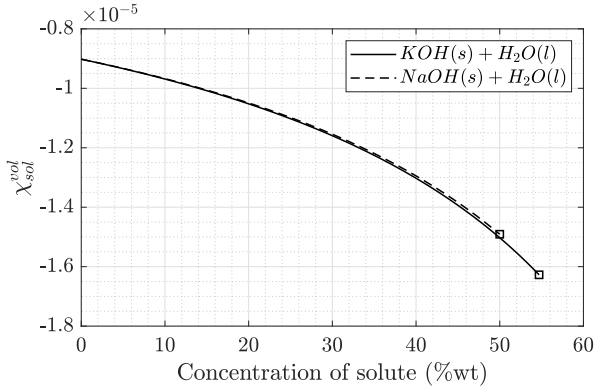

Fig. 3: Volume magnetic susceptibility of KOH and NaOH solutions as a function of the mass fraction of solute neglecting dipole interaction

32]. In consequence, understanding this process is of major importance for future applications.

The evolution of an isolated gas bubble subjected to an inhomogeneous magnetic field in microgravity can be studied as a four-step process, represented in Fig. 4: nucleation, growth, detachment, and transport. The magnetic force should not produce significant effects in the nucleation phase, but may impact the rest. Although microgravity experiments show that the actual electrolysis reaction is significantly more complicated due to the formation of a layer of bubbles and their coalescence [12–15], the tools here introduced are still useful to draw fundamental conclusions. A comprehensive chemical analysis of the bubble nucleation process can be found in Ref. 71.

4.1 Growth

The quasi-static momentum balance is one of the fundamental and most widely extended tools to study bubble growth. Let's consider

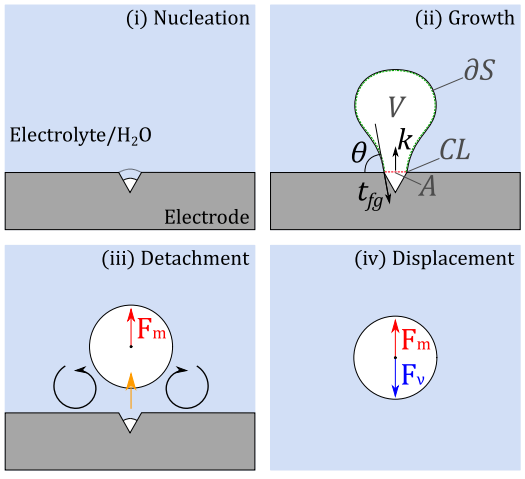

Fig. 4: Conceptual stages of single bubble evolution when subjected to an inhomogeneous magnetic field in microgravity. Detachment occurs when the vertical momentum balance is no longer satisfied, inducing a microconvection flow in the surrounding liquid. The bubble subsequently accelerates until viscous drag $\boldsymbol{F}_\nu$ compensates the magnetic buoyancy force, reaching the terminal velocity.

a liquid environment with density ρ_f and a body consisting on a single gas bubble with volume V, density ρ_g, and surface tension σ. The bubble is sitting on an horizontal electrode with apparent contact angle θ while subjected to an inertial acceleration $\boldsymbol{g}$. In the absence of dynamic forces, the momentum balance can be obtained as done in Ref. 27 for the electric interaction, resulting in

$$\int_V \mathrm{d}V \rho_g \boldsymbol{g} + \int_{CL} \mathrm{d}L \sigma \boldsymbol{t}_{fg} + \oint_{\partial V} \mathrm{d}S \; \boldsymbol{n} \cdot \mathrm{T}_p^+ + \oint_{\partial V} \mathrm{d}S \; \boldsymbol{n} \cdot \mathrm{T}_m^+ = 0, \tag{16}$$

where CL denotes the circular contact line of diameter D_0, and $\boldsymbol{t_{fg}}$ is the tangent unit vector in the meridian plane. In the above expression, $\boldsymbol{n} \cdot \mathrm{T}_p^+$ and $\boldsymbol{n} \cdot \mathrm{T}_m^+$ represent the force densities on the external face of the bubble linked to the pressure and the magnetic interaction. In quasi-static conditions, the pressure term in Eq. 16 includes the inertial and magnetic flotability forces acting on the bubble. On the other hand, for practical purposes it is useful to project Eq. 16 on the axis $\boldsymbol{k}$ perpendicular to a plane surface A delimited by CL. A scalar equilibrium equation

$$F_b + F_p + F_\sigma + F_m = 0 \tag{17}$$

is then obtained. If uniform fluid density and overpressure on A are assumed, the buoyancy, internal overpressure, and surface tension forces have the same expressions as those proposed in Ref. 27

$$F_b = \boldsymbol{k} \cdot \boldsymbol{F}_{\text{in}}^{\text{eff}} \approx V \left(\rho_g - \rho_f\right) \boldsymbol{k} \cdot \boldsymbol{g}, \tag{18}$$

$$F_p = \frac{\pi D_0^2}{4} \left(p_g - p_f^*\right), \tag{19}$$

$$F_\sigma = \int_{CL} \mathrm{d}L \sigma \boldsymbol{k} \cdot \boldsymbol{t}_{fg} \approx -\pi D_0 \sigma \sin\theta, \tag{20}$$

For water-gas solutions, with susceptibilities of the order of $|\chi^{\text{vol}}| \approx 10^{-6}$, it is appropriate to approximate the magnetic fields in Eq. 12 as $\boldsymbol{H}, \boldsymbol{H}^* \approx \boldsymbol{H_0}$. The total force exerted on a small, spherical, gas bubble is then

$$\boldsymbol{F}_m^{\text{eff}} \approx \frac{2}{3} \pi R_b^3 \mu_0 \Delta\chi^{\text{vol}} \nabla H_0^2, \tag{21}$$

where R_b is the radius of the bubble and with $\Delta\chi^{\text{vol}} = \chi_b^{\text{vol}} - \chi_e^{\text{vol}}$ denoting the differential magnetic susceptibility between gas and the water environment. This approach has been widely employed in previous works on dielectric manipulation in low-gravity [36, 37]. For the quasi-axisymmetric case, the magnetic term in Eq. 17 can be consequently approximated as

$$F_m = \boldsymbol{k} \cdot \boldsymbol{F}_m^{\text{eff}} \approx \frac{2}{3} \pi R_b^3 \mu_0 \Delta\chi^{\text{vol}} \frac{\partial H_0^2}{\partial z}. \tag{22}$$

The momentum balance may consider a forced viscous shear flow by including the viscous stress tensor and its associated lift and drag expressions [72].

4.2 Detachment

The detachment of the bubble is produced when the balance of vertical forces cannot longer be satisfied with increasing volume [26]. In this context, the magnetic force F_m can be employed to accelerate the detachment process or, equivalently, reduce the critical bubble volume.

Alternative simplified expressions can be developed to estimate the bubble detachment radius. In boiling and heat transfer research,

the maximum break-of diameter of a bubble on an upward facing surface is usually estimated form Fritz's equation [73]

$$d_0 = 1.2\theta\sqrt{\frac{\sigma}{g\left(\rho_f - \rho_g\right)}}. \tag{23}$$

If the bubble is sufficiently small, the magnetic force may be approximated by a constant, uniform field. The *magnetic Fritz equation* would then be rewritten as

$$d_0 = 1.2\theta\sqrt{\frac{\sigma}{f_m + g\left(\rho_f - \rho_g\right)}}, \tag{24}$$

with $f_m = F_m/V$ being the *overall* magnetic body force density (in N/m^3). The departure diameter may deviate from this result due to the microconvection flow associated to the detachment process [73] and the interactions between adjacent bubbles [12, 13, 15]. Furthermore, in electrolysis applications the break-of diameter also depends on the surface current density through an expression of the form [74]

$$\frac{d_b}{d_0} = \left(1 + k_1 \frac{I/A}{[A/m^{-2}]}\right)^{-k_2}, \tag{25}$$

where k_i are fitting parameters, I is the electrode current intensity, and A is the electrode effective surface area.

4.3 Displacement

The movement of a spherical bubble within a liquid can be described by the balance between buoyancy and viscous forces

$$m_b' \frac{d^2\boldsymbol{x}}{dt^2} = \boldsymbol{F}_m^{\text{eff}} + \boldsymbol{F}_{\text{in}}^{\text{eff}} + \boldsymbol{F}_R, \tag{26}$$

with $m_b' = (4/3)\pi R_b^3(\rho_g + 0.5\rho_f)$ being the virtual mass of the bubble [75], and $\boldsymbol{F}_R = -6\pi R_b\eta(d\boldsymbol{x}/dt)$ the viscous force according to Stokes' law ($Re \ll 1$). Small gas bubbles experience large initial accelerations due to their small density, rapidly reaching a steady-state regime. This justifies the employment of the *terminal velocity*, defined as the steady-state velocity of the bubble, as a physically meaningful parameter. An approximate expression of the terminal velocity can be derived from the momentum balance in Eq, 26 by neglecting the acceleration term and making use of the simplified total force expression given by Eq. 21

$$\boldsymbol{v}_t \approx \frac{2R_b^2}{9\eta}\left[\frac{\mu_0}{2}\Delta\chi^{\text{vol}}\nabla H_0^2 + \left(\rho_g - \rho_f\right)\boldsymbol{g}\right]. \tag{27}$$

The validity of this expression is limited to small bubbles and low-susceptibility gases and liquids. Similar formulations can be found in the literature [34, 36].

5 Numerical analysis

A series of numerical results are here presented to better understand low-gravity magnetic buoyancy and its applications in electrolysis and phase separation. This preliminary analysis and system sizing is made based on the previously introduced equations. For this purpose, a TDK NEOREC 62 Series (HAL) neodymium magnet, one of the strongest of its class commercially available, is considered. The magnet is characterized by a residual magnetic flux density of 1430 mT[4]. Relevant physicochemical properties of water, gas hydrogen, and gas oxygen at 25°C and 1 atm are given in Table 2.

Tab. 2: Relevant physicochemical properties of water, gas hydrogen, and gas oxygen at 25°C and 1 atm [70].

Material	$\mathcal{M}$ [g/mol]	ρ [kg/m^3]	χ^{vol}	η [Pa·s]
H_2O (l)	18.015	997	$-9.1 \cdot 10^{-6}$	0.0009
H_2 (g)	2.016	0.082	$1 \cdot 10^{-10}$	-
O_2 (g)	31.999	1.308	$3.73 \cdot 10^{-7}$	-

In order to ease the presentation of results, an expression for the effective magnetic body force distribution acting on a gas bubble submerged in a magnetic liquid is first obtained. By applying the Kelvin force density given by Eq. 8c and the Archimedes' principle as in the Sec. 3.3, one gets

$$f_m^{\text{V,eff}} = \mu_0(\chi_b^{\text{vol}} H\nabla H - \chi_e^{\text{vol}} H^*\nabla H^*). \tag{28}$$

Since low-susceptibility liquids are being considered in the analysis, the surface force density can be safely neglected [66]. The volume force density is first computed by means of finite-element simulations in Comsol Multiphysics. The equations and boundary conditions of the magnetic model are similar to the ones employed in Ref. 43. Figure 5 shows the radial cross-section of the volume force density field induced by a cylindrical magnet with 1 cm radius and 0.5 cm height on a O_2 bubble in water. Due to the small magnetic susceptibility of water, values of 1 nN/mm^3, corresponding to an inertial acceleration of ≈1 mm/s^2, are reached at 2 cm from the surface of the magnet.

Figure 6 shows the terminal velocity field (Eq. 27) of a 1 mm radius O_2 bubble immersed in water and subjected to the influence of

[4] https://product.tdk.com/info/en/catalog/datasheets/magnet_neo_summary_en.pdf, Consulted on: 10/06/2020

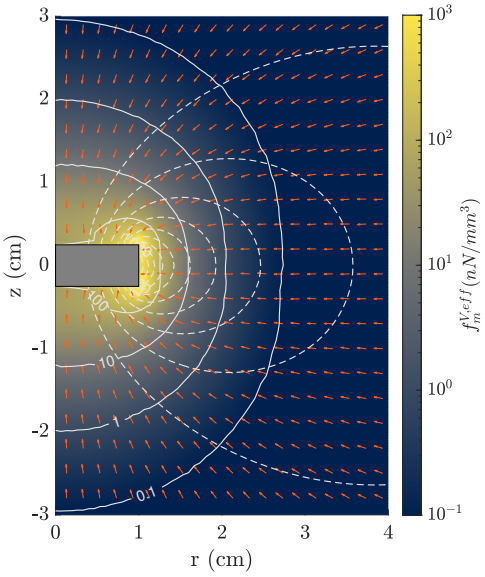

Fig. 5: Radial cross-section of the magnetic force density induced by a cylindrical magnet in an O_2 gas bubble. The red arrows, solid lines, and dashed lines represent the non-scaled force vector, the constant force contours, and the magnetic flux lines, respectively.

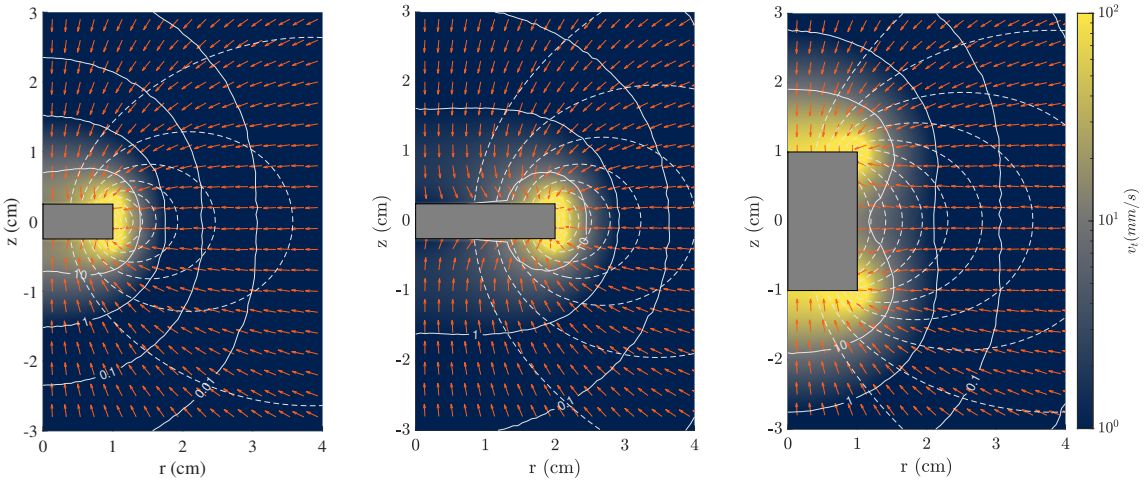

(a) Base configuration (b) Radially extended (c) Axially extended

Fig. 6: Radial cross-section of the microgravity terminal velocity v_t induced by a cylindrical magnet in an O_2 gas bubble with 1 mm radius in water. The red arrows, solid lines, and dashed lines represent the non-scaled velocity vector, the constant velocity contours, and the magnetic flux lines, respectively.

a permanent neodymium magnet in microgravity ($g \approx 0$). The red arrows, solid lines, and dashed lines correspond to the non-scaled velocity vector, the constant velocity contours, and the magnetic flux lines, respectively. Three different cylindrical magnets magnetized along the axis are studied, the first (a) with 10 mm radius and 5 mm height, the second (b) with 20 mm radius and 5 mm height, and the third (c) with 10 mm radius and 20 mm height. As expected, the velocity vectors point towards the magnets. This can be employed to induce phase separation and the detachment of gas bubbles from an electrode or a boiling surface in low-gravity. The performance of the magnets is hampered by the rapid magnetic field decay, leading to terminal velocities of the order of 1 mm/s at approximately 15 mm from their surface. Larger velocities are experienced in the corners of the magnets, where the magnetic field gradient is maximum.

The magnetic body force is proportional to the gradient of the magnetic field $\boldsymbol{H}$ and its module. When a quasi-uniform field is generated, as observed near the axis of Fig. 6b, the magnetic forces and terminal velocities are strongly reduced. It is then convenient to select a magnetic configuration that maximizes the force exerted on the bubbles. Similar problems appear in biomedical applications dealing with magnetic drug delivery and targeting [76–79] or magnetic resonance imaging [80, 81], and have been faced by means of Halbach magnet arrays. A Halbach magnet array is an arrangement of permanent magnets that reinforces the magnetic field on one side of the array and cancels it on the other [82]. These characteristics are convenient for space applications, where the performance of the magnet should be maximized, and its electromagnetic noise and mass should be minimized.

Figure 7 represents a linear array of five $1 \times 1 \times 0.5$ cm^3 neodymium magnets configured considering (a) aligned magnetizations, and (b) Halbach-oriented magnetizations. As in Fig. 6, the terminal velocity map computed with Eq. 27 is represented. It can be observed how the Halbach configuration produces an asymmetrical magnetic field and a more homogeneous terminal velocity distribution, with the 1 mm/s contour line staying at approximately 2 cm from the magnets along the x axis. However, the terminal velocity is shown to decay faster than in the linear configuration, as exemplified by the 0.1 mm/s line. This characteristic may guide the design of future phase separators. For instance, the linear configuration may be more suitable for the gas collection process due to the convergence of the velocity vectors towards the extremes of the magnet, while the Halbach array may produce a more homogeneous magnetic force distribution over the electrodes.

These results can be easily extended to the KOH or $NaOH$ solutions studied in Sec. 3.4 by noting the linear dependence of the terminal velocity with the volume magnetic susceptibility χ^{vol}. Because this parameter is a 60-80% larger than that of pure water, the performance of the system would be greatly improved. The Lorentz force would also play a significant role due to the presence of free ions, as reported in previous research [45, 46, 48, 49, 52]. Similar effects would be observed in applications involving ferrofluids, whose magnetic susceptibility can be of the order of 10. Without considering the many technical difficulties associated to their operation, such technologies could easily reach magnetic force values equal or larger than the acceleration of gravity. This may lead to large improvements in the productivity of the cell both on Earth and in space.

The influence of the magnetic field on the break-of diameter of an isolated bubble is finally explored in Fig. 8 by making use of Eq. 24. A 10 mm radius, 5 mm height cylindrical magnet is considered in microgravity, assuming a contact angle of $\theta = 5°$. The magnetic Fritz equation predicts a reduction of the break-of diameter from 10 cm to few millimeters as the bubble approaches the magnet. The employment of saturated $KOH/NaOH$ solutions would reduce the diameter by a 25% due to the increase in magnetic susceptibility, but no significant differences are observed for O_2 or H_2 gas bubbles due to their small magnetic susceptibility. These predictions should however be taken with care, as the magnetic Fritz equation assumes an homogeneous magnetic force in the bubble volume, and this assumption is being violated in a significant portion of the solution domain. Even if this was not the case, the Fritz equation describes the detachment of an isolated bubble. Experimental observations

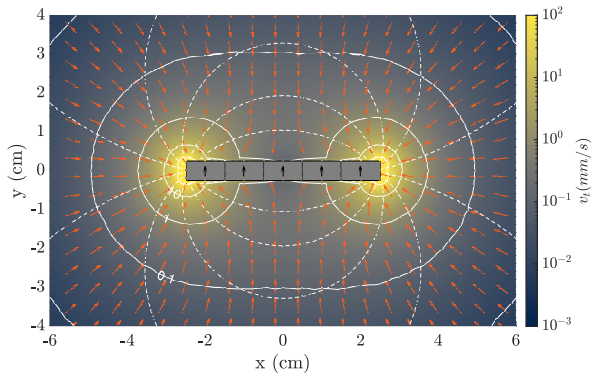

(a) Uniform magnetization

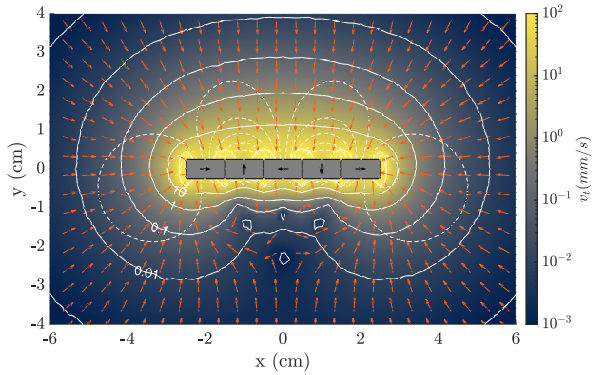

(b) Halbach array

Fig. 7: Two-dimensional simulation with 1 cm depth of the microgravity terminal velocity v_t induced by an array of magnets in an O_2 gas bubble with 1 mm radius in water. The black arrows, red arrows, solid lines, and dashed lines represent the magnetization direction, non-scaled velocity vector, the constant velocity contours, and the magnetic flux lines, respectively.

have shown that the break-of diameter in microgravity is actually much smaller due to the interaction between bubbles located in the first layer over the electrodes [12, 13, 15]. Numerical simulations

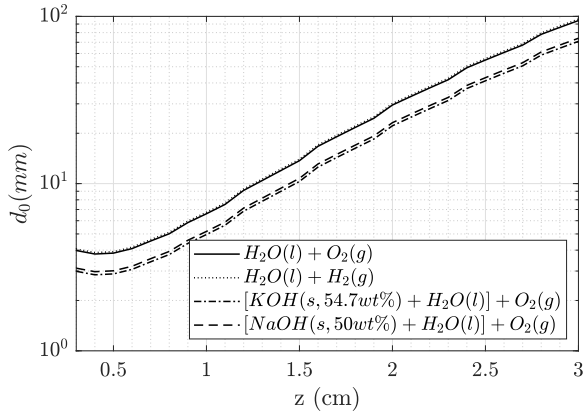

Fig. 8: Bubble break-of diameter d_0 induced by a 10 mm radius, 5 mm height cylindrical magnet in the axis of symmetry. Different gas-liquid pairs are considered with contact angle $\theta = 5°$.

based on the framework of analysis presented in Sec. 4.1 and experimental results would be required to shed light on this problem.

6 Conclusions

The applications of magnetic buoyancy in low-gravity electrolysis, boiling, and phase separation have been introduced. The magnetic force would induce the early detachment of gas bubbles from the electrodes, increasing the effective surface area and separating the phases. A comprehensive theoretical analysis of the problem has been presented together with simplified expressions that ease preliminary studies.

Fundamental results are employed to show how modern centimeter-size neodymium magnets induce a significant magnetic force in gas-water flows at distances of the order of 2 cm. The reachability of the system is increased by a 80% when saturated $NaOH$ and KOH electrolytes are considered. Future applications may explore the use of ferrofluids, which exhibit larger magnetic susceptibilities and a strong magnetic response. This would lead to significant increases of the magnetic force, also enabling terrestrial applications.

There are several scientific and technical questions of interest that need to be solved before magnetic buoyancy is employed in low-gravity technologies. A non extensive list includes studies of the uncertainty in the bubble collection process, the experimental and numerical study of magnetically-induced bubble detachment, the development of reliable gas sinks, or the analysis of applications employing ferrofluids, among others.

7 Acknowledgments

The project leading to these results has received funding from *la Caixa* Foundation (ID 100010434), under agreement LCF/BQ/AA18/11680099.

References

[1] R. de Levie. “The electrolysis of water”. In: *Journal of Electroanalytical Chemistry* 476.1 (1999), pp. 92–93. ISSN: 1572-6657. DOI: https://doi.org/10.1016/S0022-0728(99)00365-4.

[2] S Trasatti. “Water electrolysis: who first?” In: *Journal of Electroanalytical Chemistry* 476.1 (1999), pp. 90–91. ISSN: 1572-6657. DOI: https://doi.org/10.1016/S0022-0728(99)00364-2.

[3] D. Newman. “Water electrolysis reaction control system”. In: *Proc. of the 7th Liquid Propulsion Symposium, Chemical Propulsion Information Agency Publications*. Vol. 72. Oct. 1965, pp. 105–114.

[4] Robert Roy. “Backwards Runs the Reaction”. In: *Mechanical Engineering* 130.04 (Apr. 2008), pp. 32–36. ISSN: 0025-6501. DOI: 10.1115/1.2008-APR-3.

[5] William Papale and Robert Roy. “A Water-Based Propulsion System for Advanced Spacecraft”. In: *Space 2006*. 2006, pp. 1–13. DOI: 10.2514/6.2006-7240.

[6] K. James, T. Moser, A. Conley, J. Slostad, and R. Hoyt. “Performance Characterization of the HYDROS Water Electrolysis Thruster”. In: *Proc. of the Small Satellite Conference 2015. Paper SSC15-XI-5*. 2015, pp. 1–7.

[7] K. P. Doyle and M. A. Peck. "Water Electrolysis Propulsion as a Case Study in Resource-Based Spacecraft Architecture (February 2020)". In: *IEEE Aerospace and Electronic Systems Magazine* 34.9 (2019), pp. 4–19.

[8] K.A. Burke. "Small Portable PEM Fuel Cell Systems for NASA Exploration Missions". In: *NASA Technical Report TM-2005-213994* (2005).

[9] D.J. Bents, V.J. Scullin, B.J. Chang, D.W. Johnson, and C.P. García snf I.J. Jakupca. "Hydrogen-Oxygen PEM Regenerative Fuel Cell Development at the NASA Glenn Research Center". In: *NASA Technical Report TM-2005-214032* (2005).

[10] K.A. Lee. "Water electrolysis for in-situ resource utilization (ISRU)". In: *AIAA Houston Section Annual Technical Symposium (ATS 2016)*. 2016.

[11] George F. Sowers and Christopher B. Dreyer. "Ice Mining in Lunar Permanently Shadowed Regions". In: *New Space* 7.4 (2019), pp. 235–244. DOI: 10.1089/space.2019.0002.

[12] H Matsushima, T Nishida, Y Konishi, Y Fukunaka, Y Ito, and K Kuribayashi. "Water electrolysis under microgravity: Part 1. Experimental technique". In: *Electrochimica Acta* 48.28 (2003), pp. 4119–4125. ISSN: 0013-4686. DOI: https://doi.org/10.1016/S0013-4686(03)00579-6.

[13] H. Matsushima, Y. Fukunaka, and K. Kuribayashi. "Water electrolysis under microgravity: Part II. Description of gas bubble evolution phenomena". In: *Electrochimica Acta* 51.20 (2006), pp. 4190–4198. ISSN: 0013-4686. DOI: https://doi.org/10.1016/j.electacta.2005.11.046.

[14] Daisuke Kiuchi, Hisayoshi Matsushima, Yasuhiro Fukunaka, and Kazuhiko Kuribayashi. "Ohmic Resistance Measurement of Bubble Froth Layer in Water Electrolysis under Microgravity". In: *Journal of The Electrochemical Society* 153.8 (2006), E138. DOI: 10.1149/1.2207008.

[15] A. Iwasaki, H. Kaneko, Y. Abe, and M. Kamimoto. "Investigation of electrochemical hydrogen evolution under microgravity condition". In: *Electrochimica Acta* 43.5 (1998), pp. 509–514. ISSN: 0013-4686. DOI: https://doi.org/10.1016/S0013-4686(97)00096-0.

[16] Masato Sakurai, Asuka Shima, Yoshitsugu Sone, Mitsuru Ohnishi, Satoru Tachihara, and Tsuyoshi Ito. "Development of Oxygen Generation Demonstration on JEM (KIBO) for Manned Space Exploration". In: *44th International Conference on Environmental Systems, Tucson, Arizona*. July 2014, pp. 1–7.

[17] Robert J. Erickson, John Howe, Galen W. Kulp, and Steven P. Van Keuren. "International Space Station United States Orbital Segment Oxygen Generation System On-orbit Operational Experience". In: *International Conference On Environmental Systems, 2008-01-1962*. June 2008. DOI: https://doi.org/10.4271/2008-01-1962.

[18] Darren J. Samplatsky and W. Clark Dean. "Development of a Rotary Separator Accumulator for Use on the International Space Station". In: *International Conference On Environmental Systems*. SAE International, July 2002. DOI: https://doi.org/10.4271/2002-01-2360.

[19] Masato Sakurai, Takuma Terao, and Yoshitsugu Sone. "Development of Water Electrolysis System for Oxygen Production Aimed at Energy Saving and High Safety". In: *45th International Conference on Environmental Systems, Belleuve, Washington*. July 2015, pp. 1–8.

[20] Ryan M. Jenson, Andrew P. Wollman, Mark M. Weislogel, Lauren Sharp, Robert Green, Peter J. Canfield, Jörg Klatte, and Michael E. Dreyer. "Passive phase separation of microgravity bubbly flows using conduit geometry". In: *International Journal of Multiphase Flow* 65 (2014), pp. 68–81. ISSN: 0301-9322. DOI: https://doi.org/10.1016/j.ijmultiphaseflow.2014.05.011.

[21] Mark M. Weislogel and Joshua T. McCraney. "The symmetric draining of capillary liquids from containers with interior corners". In: *Journal of Fluid Mechanics* 859 (2019), pp. 902–920. DOI: 10.1017/jfm.2018.848.

[22] Negar Beheshti Pour and David B. Thiessen. "A novel arterial Wick for gas–liquid phase separation". In: *AIChE Journal* 65.4 (2019), pp. 1340–1354. DOI: 10.1002/aic.16499.

[23] Negar Beheshti Pour and David B. Thiessen. "Equilibrium configurations of drops or bubbles in an eccentric annulus". In: *Journal of Fluid Mechanics* 863 (2019), pp. 364–385. DOI: 10.1017/jfm.2018.1010.

[24] D. Chipchark. *Development of expulsion and orientation systems for advanced liquid rocket propulsion systems*. 1963.

[25] P. Di Marco and W. Grassi. "Effect of force fields on pool boiling flow patterns in normal and reduced gravity". In: *Heat and Mass Transfer* 45.7 (May 2009), pp. 959–966. ISSN: 1432-1181. DOI: 10.1007/s00231-007-0328-6.

[26] Paolo Di Marco. "Influence of Force Fields and Flow Patterns on Boiling Heat Transfer Performance: A Review". In: *Journal of Heat Transfer* 134.3 (Jan. 2012). 030801. ISSN: 0022-1481. DOI: 10.1115/1.4005146.

[27] Paolo Di Marco. "The Use of Electric Force as a Replacement of Buoyancy in Two-phase Flow". In: *Microgravity Science and Technology* 24.3 (June 2012), pp. 215–228. ISSN: 1875-0494. DOI: 10.1007/s12217-012-9312-y.

[28] Rong Ma, Xiaochen Lu, Chao Wang, Chen Yang, and Wei Yao. "Numerical simulation of bubble motions in a coaxial annular electric field under microgravity". In: *Aerospace Science and Technology* 96 (2020), p. 105525. ISSN: 1270-9638. DOI: https://doi.org/10.1016/j.ast.2019.105525.

[29] Donald W. Holder, Edward W. O'Connor, John Zagaja, and Karen Murdoch. "Investigation into the Performance of Membrane Separator Technologies used in the International Space Station Regenerative Life Support Systems: Results and Lessons Learned". In: *31st International Conference On Environmental Systems*. SAE International, July 2001, pp. 1–14. DOI: https://doi.org/10.4271/2001-01-2354.

[30] L.D. Landau and E.M. Lifshitz. *Electrodynamics of Continuous Media*. Pergamon Press, 1960.

[31] Liu Junhong, Gu Jianming, Lian Zhiwei, and Liu Hui. "Experiments and mechanism analysis of pool boiling heat transfer enhancement with water-based magnetic fluid". In: *Heat and Mass Transfer* 41.2 (Dec. 2004), pp. 170–175. ISSN: 1432-1181. DOI: 10.1007/s00231-004-0529-1.

[32] Ali Abdollahi, Mohammad Reza Salimpour, and Nasrin Etesami. "Experimental analysis of magnetic field effect on the pool boiling heat transfer of a ferrofluid". In: *Applied Thermal Engineering* 111 (2017), pp. 1101–1110. ISSN: 1359-4311. DOI: https://doi.org/10.1016/j.applthermaleng.2016.10.019.

[33] Nobuko I. Wakayama. "Magnetic buoyancy force acting on bubbles in nonconducting and diamagnetic fluids under microgravity". In: *Journal of Applied Physics* 81.7 (1997), pp. 2980–2984. DOI: 10.1063/1.364330.

[34] Nobuko I. Wakayama. "Utilization of magnetic force in space experiments". In: *Advances in Space Research* 24.10 (1999). Gravitational Effects in Materials and Fluid Sciences, pp. 1337–1340. ISSN: 0273-1177. DOI: https://doi.org/10.1016/S0273-1177(99)00743-7.

[35] Brian J. Tillotson, Larry P. Torre, and Janice D. Houston. *Method for Manipulation of Diamagnetic Objects in a Low-Gravity Environment*. US Patent 6162364. 2000.

[36] E. Scarl and J. Houston. "Two-phase magnetic fluid manipulation in microgravity environments". In: *Proceedings of the 37th Aerospace Sciences Meeting and Exhibit*. 1999, pp. 1–5. DOI: 10.2514/6.1999-844.

[37] Brian Tillotson, J. Houston, Brian Tillotson, and J. Houston. "Diamagnetic manipulation for microgravity processing". In: *Proceedings of the 35th Aerospace Sciences Meeting and Exhibit*. 1997, pp. 1–10. DOI: 10.2514/6.1997-887.

[38] S.S. Papell. *Low viscosity magnetic fluid obtained by the colloidal suspension of magnetic particles*. US Patent 3215572. 1963.

[39] J.J. Martin and J.B. Holt. *Magnetically Actuated Propellant Orientation Experiment, Controlling fluid Motion With Magnetic Fields in a Low-Gravity Environment*. TM-2000-210129, M-975, NAS 1.15:210129. NASA, 2000.

[40] Jeffrey G. Marchetta. "Simulation of LOX reorientation using magnetic positive positioning". In: *Microgravity - Science and Technology* 18.1 (Mar. 2006), p. 31. ISSN: 1875-0494.

[41] J.G. Marchetta and A.P. Winter. "Simulation of magnetic positive positioning for space based fluid management systems". In: *Mathematical and Computer Modelling* 51.9 (2010), pp. 1202–1212.

[42] Á. Romero-Calvo, F. Maggi, and H. Schaub. "Prospects and challenges for magnetic propellant positioning in low-gravity". In: *Proceedings of the AAS Guidance, Navigation and Control Conference, Breckenridge, Colorado*. 2020, pp. 1–19.

[43] Álvaro Romero-Calvo, Gabriel Cano Gómez, Elena Castro-Hernández, and Filippo Maggi. "Free and Forced Oscillations of Magnetic Liquids Under Low-Gravity Conditions". In: *Journal of Applied Mechanics* 87.2 (Dec. 2019), pp. 021–010. ISSN: 0021-8936.

[44] Á. Romero-Calvo, A.J. García-Salcedo, F. Garrone, I. Rivoalen, G. Cano-Gómez, E. Castro-Hernández, M.Á. [Herrada Gutiérrez], and F. Maggi. "StELIUM: A student experiment to investigate the sloshing of magnetic liquids in microgravity". In: *Acta Astronautica* 173 (2020), pp. 344–355. ISSN: 0094-5765. DOI: https://doi.org/10.1016/j.actaastro.2020.04.013.

[45] Jakub Adam Koza, Sascha Mühlenhoff, Piotr Żabiński, Petr A. Nikrityuk, Kerstin Eckert, Margitta Uhlemann, Annett Gebert, Tom Weier, Ludwig Schultz, and Stefan Odenbach. "Hydrogen evolution under the influence of a magnetic field". In: *Electrochimica Acta* 56.6 (2011), pp. 2665–2675. ISSN: 0013-4686. DOI: https://doi.org/10.1016/j.electacta.2010.12.031.

[46] Mingyong Wang, Zhi Wang, Xuzhong Gong, and Zhancheng Guo. "The intensification technologies to water electrolysis for hydrogen production – A review". In: *Renewable and Sustainable Energy Reviews* 29 (2014), pp. 573–588. ISSN: 1364-0321. DOI: https://doi.org/10.1016/j.rser.2013.08.090.

[47] Ming-Yuan Lin, Lih-Wu Hourng, and Chan-Wei Kuo. "The effect of magnetic force on hydrogen production efficiency in water electrolysis". In: *International Journal of Hydrogen Energy* 37.2 (2012). 10th International Conference on Clean Energy 2010, pp. 1311–1320. ISSN: 0360-3199. DOI: https://doi.org/10.1016/j.ijhydene.2011.10.024.

[48] Ming Yuan Lin and Lih Wu Hourng. "Effects of magnetic field and pulse potential on hydrogen production via water electrolysis". In: *International Journal of Energy Research* 38.1 (2014), pp. 106–116. DOI: 10.1002/er.3112.

[49] Ming Yuan Lin, Lih Wu Hourng, and Ja Shen Hsu. "The effects of magnetic field on the hydrogen production by multielectrode water electrolysis". In: *Energy Sources, Part A: Recovery, Utilization, and Environmental Effects* 39.3 (2017), pp. 352–357. DOI: 10.1080/15567036.2016.1217289.

[50] Mehmet Fatih Kaya, Nesrin Demir, M. Salahaldin Albawabiji, and Mert Taş. "Investigation of alkaline water electrolysis performance for different cost effective electrodes under magnetic field". In: *International Journal of Hydrogen Energy* 42.28 (2017). Special Issue on The 4th European Conference on Renewable Energy Systems (ECRES 2016), 28-31 August 2016, Istanbul, Turkey, pp. 17583–17592. ISSN: 0360-3199. DOI: https://doi.org/10.1016/j.ijhydene.2017.02.039.

[51] Noriah Bidin, Siti Radhiana Azni, Shumaila Islam, Mundzir Abdullah, M. Fakaruddin Sidi Ahmad, Ganesan Krishnan, A. Rahman Johari, M. Aizat A. Bakar, Nur Syahirah Sahidan, NurFatin Musa, M. Farizuddin Salebi, Naqiuddin Razali, and Mohd Marsin Sanagi. "The effect of magnetic and optic field in water electrolysis". In: *International Journal of Hydrogen Energy* 42.26 (2017), pp. 16325–16332. ISSN: 0360-3199. DOI: https://doi.org/10.1016/j.ijhydene.2017.05.169.

[52] Felipe A. Garcés-Pineda, Marta Blasco-Ahicart, David Nieto-Castro, Núria López, and José Ramón Galán-Mascarós. "Direct magnetic enhancement of electrocatalytic water oxidation in alkaline media". In: *Nature Energy* 4.6 (June 2019), pp. 519–525. ISSN: 2058-7546. DOI: 10.1038/s41560-019-0404-4.

[53] Yang Liu, Liang-ming Pan, Hongbo Liu, Tianming Chen, Siyou Yin, and Mengmeng Liu. "Effects of magnetic field on water electrolysis using foam electrodes". In: *International Journal of Hydrogen Energy* 44.3 (2019), pp. 1352–1358. ISSN: 0360-3199. DOI: https://doi.org/10.1016/j.ijhydene.2018.11.103.

[54] Hong-bo Liu, Haotian Xu, Liang-ming Pan, Ding-han Zhong, and Yang Liu. "Porous electrode improving energy efficiency under electrode-normal magnetic field in water electrolysis". In: *International Journal of Hydrogen Energy* 44.41 (2019), pp. 22780–22786. ISSN: 0360-3199. DOI: https://doi.org/10.1016/j.ijhydene.2019.07.024.

[55] Purnami, Nurkholis Hamidi, Mega Nur Sasongko, Denny Widhiyanuriyawan, and I.N.G. Wardana. "Strengthening external magnetic fields with activated carbon graphene for increasing hydrogen production in water electrolysis". In: *International Journal of Hydrogen Energy* (2020). ISSN: 0360-3199. DOI: https://doi.org/10.1016/j.ijhydene.2020.05.148.

[56] P. Millet and S. Grigoriev. "Chapter 2 - Water Electrolysis Technologies". In: *Renewable Hydrogen Technologies*. Ed. by Luis M. Gandía, Gurutze Arzamendi, and Pedro M. Diéguez. Amsterdam: Elsevier, 2013, pp. 19–41. ISBN: 978-0-444-56352-1. DOI: https://doi.org/10.1016/B978-0-444-56352-1.00002-7.

[57] F.H. Schubert. "Electrolysis Performance Improvement Concept Study (EPICS) Flight Experiment-Reflight". In: *NASA Technical Report CR-205554, TR-1415-57* (1997).

[58] N. M. Samsonov, L. S. Bobe, L. I. Gavrilov, V. P. Korolev, V. M. Novikov, N. S. Farafonov, V. A. Soloukhin, S. Ju. Romanov, P. O. Andrejchuk, N. N. Protasov, A. M. Rjabkin, A. A. Telegin, Ju. E. Sinjak, and V. M. Skuratov. "Water Recovery and Oxygen Generation by Electrolysis Aboard the International Space Station". In: *International Conference On Environmental Systems*. SAE International, July 2002. DOI: https://doi.org/10.4271/2002-01-2358.

[59] Kevin Takada, Luis E. Velasquez, Steven Van Keuren, Phillip S. Baker, and Stephen H. McDougle. "Advanced Oxygen Generation Assembly for Exploration Missions". In: *49th International Conference On Environmental Systems, Boston, Massachusetts*. July 2019.

[60] Mohammed Saad Kamel and Ferenc Lezsovits. "Enhancement of pool boiling heat transfer performance using dilute cerium oxide/water nanofluid: An experimental investigation". In: *International Communications in Heat and Mass Transfer* 114 (2020), p. 104587. ISSN: 0735-1933. DOI: https://doi.org/10.1016/j.icheatmasstransfer.2020.104587.

[61] Ashkan Vatani, Peter Lloyd Woodfield, Toan Dinh, Hoang-Phuong Phan, Nam-Trung Nguyen, and Dzung Viet Dao. "Degraded boiling heat transfer from hotwire in ferrofluid due to particle deposition". In: *Applied Thermal Engineering* 142 (2018), pp. 255–261. ISSN: 1359-4311. DOI: https://doi.org/10.1016/j.applthermaleng.2018.06.064.

[62] Ronald E. Rosensweig. "Stress Boundary-Conditions in Ferrohydrodynamics". In: *Industrial & Engineering Chemistry Research* 46.19 (2007), pp. 6113–6117. DOI: 10.1021/ie060657e.

[63] A. Engel and R. Friedrichs. "On the electromagnetic force on a polarizable body". In: *American Journal of Physics* 70.4 (2002), pp. 428–432.

[64] Ronald E. Rosensweig. "Continuum equations for magnetic and dielectric fluids with internal rotations". In: *The Journal of Chemical Physics* 121.3 (2004), pp. 1228–1242. DOI: 10.1063/1.1755660.

[65] R. E. Rosensweig. *Ferrohydrodynamics*. Dover Publications, 1997.

[66] Á. Romero-Calvo, Gabriel Cano-Gómez, Tim H.J. Hermans, Lidia Parrilla Benítez, Miguel Ángel Herrada Gutiérrez, and Elena Castro-Hernández. "Total magnetic force on a ferrofluid droplet in microgravity". In: *Experimental Thermal and Fluid Science* (2020), p. 110124. ISSN: 0894-1777.

[67] P.W. Kuchel, B.E. Chapman, W.A. Bubb, P.E. Hansen, C.J. Durrant, and M.P. Hertzberg. "Magnetic susceptibility: Solutions, emulsions, and cells". In: *Concepts in Magnetic Resonance Part A* 18A.1 (2003), pp. 56–71. DOI: 10.1002/cmr.a.10066.

[68] William F Pickering. *Modern analytical chemistry*. New York-Dekker, 1971.

[69] Gordon A. Bain and John F. Berry. "Diamagnetic Corrections and Pascal's Constants". In: *Journal of Chemical Education* 85.4 (2008), p. 532. DOI: 10.1021/ed085p532.

[70] D. R. Lide. *CRC Handbook of Chemistry and Physics: 84th Edition*. CRC Press, 2003. ISBN: 9780849304811.

[71] Andrea Angulo, Peter [van der Linde], Han Gardeniers, Miguel Modestino, and David [Fernández Rivas]. "Influence of Bubbles on the Energy Conversion Efficiency of Electrochemical Reactors". In: *Joule* 4.3 (2020), pp. 555–579. ISSN: 2542-4351. DOI: https://doi.org/10.1016/j.joule.2020.01.005.

[72] Géraldine Duhar and Catherine Colin. "Dynamics of bubble growth and detachment in a viscous shear flow". In: *Physics of Fluids* 18.7 (2006), p. 077101. DOI: 10.1063/1.2213638.

[73] Karl Stephan. "Physical Fundamentals of Vapor Bubble Formation". In: *Heat Transfer in Condensation and Boiling*. Berlin, Heidelberg: Springer Berlin Heidelberg, 1992, pp. 126–139. ISBN: 978-3-642-52457-8. DOI: 10.1007/978-3-642-52457-8_10.

[74] H. Vogt and R.J. Balzer. "The bubble coverage of gas-evolving electrodes in stagnant electrolytes". In: *Electrochimica Acta* 50.10 (2005), pp. 2073–2079. ISSN: 0013-4686. DOI: https://doi.org/10.1016/j.electacta.2004.09.025.

[75] L.D. Landau and E.M. Lifshitz. "Chapter I - Ideal Fluids". In: *Fluid Mechanics (Second Edition)*. Ed. by L.D. LANDAU and E.M. LIFSHITZ. Second Edition. Pergamon, 1987, pp. 30–31. ISBN: 978-0-08-033933-7. DOI: https://doi.org/10.1016/B978-0-08-033933-7.50009-X.

[76] A. Sarwar, A. Nemirovski, and B. Shapiro. "Optimal Halbach Permanent Magnet Designs for Maximally Pulling and Pushing Nanoparticles". In: *Journal of magnetism and magnetic materials* 324.5 (Mar. 2012). 23335834[pmid], pp. 742–754. ISSN: 0304-8853. DOI: 10.1016/j.jmmm.2011.09.008.

[77] B. Shapiro, S. Kulkarni, A. Nacev, A. Sarwar, D. Preciado, and D.A. Depireux. "Shaping Magnetic Fields to Direct Therapy to Ears and Eyes". In: *Annual Review of Biomedical Engineering* 16.1 (2014). PMID: 25014789, pp. 455–481. DOI: 10.1146/annurev-bioeng-071813-105206.

[78] Lester C Barnsley, Dario Carugo, Joshua Owen, and Eleanor Stride. "Halbach arrays consisting of cubic elements optimised for high field gradients in magnetic drug targeting applications". In: *Physics in Medicine and Biology* 60.21 (Oct. 2015), pp. 8303–8327. DOI: 10.1088/0031-9155/60/21/8303.

[79] Mahendran Subramanian, Arkadiusz Miaskowski, Stuart Iain Jenkins, Jenson Lim, and Jon Dobson. "Remote manipulation of magnetic nanoparticles using magnetic field gradient to promote cancer cell death". In: *Applied Physics A* 125.4 (Mar. 2019), p. 226. ISSN: 1432-0630. DOI: 10.1007/s00339-019-2510-3.

[80] Ashvin Bashyam, Matthew Li, and Michael J. Cima. "Design and experimental validation of Unilateral Linear Halbach magnet arrays for single-sided magnetic resonance". In: *Journal of Magnetic Resonance* 292 (2018), pp. 36–43. ISSN: 1090-7807. DOI: https://doi.org/10.1016/j.jmr.2018.05.004.

[81] Clarissa Zimmerman Cooley, Melissa W. Haskell, Stephen F. Cauley, Charlotte Sappo, Cristen D. Lapierre, Christopher G. Ha, Jason P. Stockmann, and Lawrence L. Wald. "Design of sparse Halbach magnet arrays for portable MRI using a genetic algorithm". In: *IEEE Transactions on Magnetics* 54.1 (Jan. 2018), p. 5100112. ISSN: 0018-9464.

[82] K. Halbach. "Design of permanent multipole magnets with oriented rare earth cobalt material". In: *Nuclear Instruments and Methods* 169.1 (1980), pp. 1–10. ISSN: 0029-554X. DOI: https://doi.org/10.1016/0029-554X(80)90094-4.